Target selectivity of septal cholinergic neurons in the medial and lateral entorhinal cortex

Srinidhi Desikan[a,b,1], David E. Koser[a,c,1], Angela Neitz[a,c,2], and Hannah Monyer[a,c,3]

[a]Department of Clinical Neurobiology, German Cancer Research Center, 69120 Heidelberg, Germany; [b]Faculty of Biosciences, Heidelberg University, 69120 Heidelberg, Germany; and [c]Department of Clinical Neurobiology, Medical Faculty, Heidelberg University, 69120 Heidelberg, Germany

Edited by Nathaniel Heintz, The Rockefeller University, New York, NY, and approved January 31, 2018 (received for review September 20, 2017)

The entorhinal cortex (EC) plays a pivotal role in processing and conveying spatial information to the hippocampus. It has long been known that EC neurons are modulated by cholinergic input from the medial septum. However, little is known as to how synaptic release of acetylcholine affects the different cell types in EC. Here we combined optogenetics and patch-clamp recordings to study the effect of cholinergic axon stimulation on distinct neurons in EC. We found dense cholinergic innervations that terminate in layer I and II (LI and LII). Light-activated stimulation of septal cholinergic projections revealed differential responses in excitatory and inhibitory neurons in LI and LII of both medial and lateral EC. We observed depolarizing responses mediated by nicotinic and muscarinic receptors primarily in putative serotonin receptor ($p5HT_3R$)-expressing interneurons. Hyperpolarizing muscarinic receptor-mediated responses were found predominantly in excitatory cells. Additionally, some excitatory as well as a higher fraction of inhibitory neurons received mono- and/or polysynaptic GABAergic inputs, revealing that medial septum cholinergic neurons have the capacity to corelease GABA alongside acetylcholine. Notably, the synaptic effects of acetylcholine were similar in neurons of both medial and lateral EC. Taken together, our findings demonstrate that EC activity may be differentially modulated via the activation or the suppression of distinct subsets of LI and LII neurons by the septal cholinergic system.

medial septum | optogenetics | nicotinic receptor | muscarinic receptor | neurotransmitter corelease

The superficial layers of entorhinal cortex (EC) play a quintessential role in processing and conveying sensory information from the neocortex to the hippocampus via the perforant and temporoammonic pathways (1, 2). Commonly, EC is subdivided into medial EC (MEC) and lateral EC (LEC), which display both functional and organizational differences (3–5). MEC conveys mostly spatial information (6, 7), while LEC mediates nonspatial inputs to the hippocampus (8–10). Based on anatomical and electrophysiological studies, distinct principal cell types have been described in layer II (LII) of MEC and LEC (11–14). These principal cell types, together with local interneurons, constitute the complex local microcircuit in LII of EC (13, 15), which received increasing attention ever since the discovery of grid cells and other spatially tuned cells in the superficial layers of MEC (6, 7). In vivo recordings from this area in freely moving animals reveals that the most striking rhythmic activity is theta oscillations (4–12 Hz) (16), which is a prerequisite for the temporal organization of neurons within local networks. Of note, MEC exhibits stronger theta rhythmicity than LEC, and so far, it appears that in contrast to MEC, neurons in LEC are only weakly modulated by theta (17). Although local networks can support the generation and maintenance of theta oscillations (18, 19), the main source for theta oscillations in EC is the medial septum/vertical limb of the diagonal band of Broca (MS/DBB) (19–21).

It has been known for decades that MS/DBB, which is a part of the basal forebrain complex, is the main external pacemaker of hippocampal-EC theta rhythm, thereby coordinating several distant brain areas (19, 22). Pharmacological inactivation of MS strongly reduces theta oscillations and grid cell firing in MEC, leading to spatial memory deficits (23–25). The septo-entorhinal pathway comprises glutamatergic, GABAergic, and cholinergic projections (26). The target selectivity of septal glutamatergic and GABAergic projections in LII of MEC has been previously studied. While the former targets pyramidal cells (PCs) and fast-spiking (FS) interneurons (27), the latter selectively inhibits interneurons in LII of MEC (13, 28). Selective lesions of septal cholinergic neurons or their optogenetic activation have indicated that acetylcholine (ACh) plays an important role in regulating theta rhythmic activity in the hippocampus, thereby augmenting the dynamics of memory encoding (29–32). Optogenetic activation of septal cholinergic fibers in the CA1 region of the hippocampus evoked responses in both PCs and in a variety of interneurons (33–35), but the identity of cholinergic MS/DBB target cells in EC has remained elusive. In vitro investigations using bath application of cholinergic receptor agonists (36, 37) gave first indications as to differential effects of ACh in EC neurons. However, technical limitations precluded specific axonal activation that is nowadays offered by virus-supported optogenetics, enabling both clear-cut identification of source cells and mimicking of endogenous release.

Here we analyzed the septal cholinergic projections to MEC and LEC, focusing on the identification of target cells and characterization of optogenetically induced responses. We characterized the projections based on antero- and retrograde tracing. Following virus-mediated *ChR2-mCherry* expression in cholinergic MS/DBB neurons, we electrophysiologically studied cholinergic

Significance

Acetylcholine is a key modulator of hippocampal and entorhinal cortex (EC) function. The majority of cholinergic projections targeting these structures originate in the basal forebrain complex, specifically the medial septum. Many studies focused on the behavioral effects involving these projections, but there still is a paucity regarding their connectivity in the target area. Here we provide this missing link. By combining optogenetics with whole-cell recordings in superficial EC layers, we identified the synaptic target cells of septal cholinergic neurons. This level of analysis is an important step toward a better understanding of the modulatory action of acetylcholine in EC in vivo.

Author contributions: H.M. conceived the research; S.D. and D.E.K. designed and performed the experiments; A.N. performed pilot experiments; D.E.K. wrote the MATLAB scripts; S.D. and D.E.K. analyzed the data; and S.D., D.E.K., and H.M. wrote the manuscript.

The authors declare no conflict of interest.

This article is a PNAS Direct Submission.

[1]S.D. and D.E.K. contributed equally to this work.

[2]Present address: Quality Department Spiriva, Böhringer Ingelheim, 55216 Ingelheim am Rhein, Germany.

[3]To whom correspondence should be addressed. Email: h.monyer@dkfz-heidelberg.de.

This article contains supporting information online at www.pnas.org/lookup/suppl/doi:10.1073/pnas.1716531115/-/DCSupplemental.

Published online February 27, 2018.

responses in identified neurons in acute slices and demonstrate that they activate or suppress distinct subsets of LI/LII neurons. Measurements in MEC and LEC were directed toward answering the question of whether common connectivity rules hold true in the two brain areas. This indeed appears to be the case. However, based on our anatomical and electrophysiological data, we infer that cell type-specific septal cholinergic modulation is more pronounced in MEC than in LEC neurons.

Results

Septal Cholinergic Neurons Project to the MEC and LEC. To investigate the extent of MS/DBB cholinergic projections to EC, we injected AAV-DIO-*ChR2-mCherry* virus (in four instances AAV-DIO-*eGFP* virus was used; for details see *SI Materials and Methods*) into MS/DBB of 8-wk-old male ChAT^{Cre} mice (Fig. 1*A*). Viral expression, as indicated by mCherry labeling of cell bodies, was observed across MS/DBB (Fig. 1*B*), with an infection rate of 50.76 ± 2.32% within MS/DBB cholinergic cells (Fig. 1*C*, 573 double$^+$ cells from a total of 1,148 ChAT$^+$ cells in 12 slices from 4 mice). We found that mCherry was virtually exclusive in MS/DBB cholinergic neurons, as 98.92 ± 0.22% of the cells positive for mCherry expression were also ChAT$^+$ (Fig. 1*C*, 573 double$^+$ cells from a total of 579 mCherry$^+$ cells in 12 slices from 4 mice). Furthermore, within MEC and LEC, we observed mCherry$^+$ cholinergic axons predominantly in LI/LII, with fewer axons in LEC (Fig. 1*G* and Fig. S1). To corroborate the results of our anterograde tracing experiments and to estimate the percentage of EC projecting septal cholinergic neurons, we injected the retrograde tracer fluorogold (FG; 0.5%) unilaterally into MEC and LEC (Fig. 1*D*). We found more MS/DBB cholinergic neurons projecting to MEC (5.70 ± 0.75%) than LEC (3.37 ± 0.51%) (Fig. 1 *E* and *F*, 93 double$^+$ cells from a total of 1,786 ChAT$^+$ cells in 14 slices from 5 mice for MEC and 83 double$^+$ cells from a total of 2,270 ChAT$^+$ cells in 15 slices from 6 mice for LEC; $P < 0.05$). As indicated by vesicular acetylcholine transporter (vAChT) stainings, the mCherry$^+$ axons within the EC can pack and release ACh (Fig. 1*H*). To test whether there is a difference in synapse density, we quantified the number of vAChT

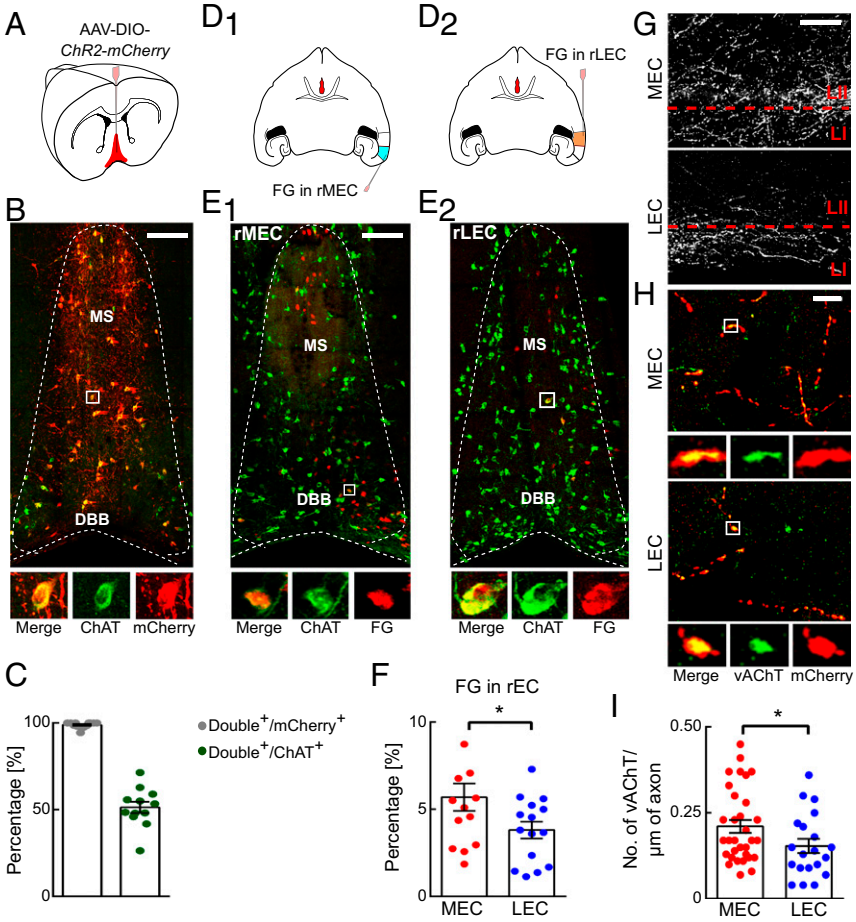

Fig. 1. MS/DBB cholinergic neurons project to EC. (*A*) Schematic representation indicating the injection site (red) in MS/DBB of a ChAT^{Cre} mouse for anterograde tracing experiments with AAV-DIO-*ChR2-mCherry*. (*B*) Maximum intensity confocal image showing selective expression of ChR2-mCherry in ChAT-expressing neurons upon stereotaxic virus injection into MS/DBB. Higher magnification of a representative mCherry$^+$/ChAT$^+$ cell from the boxed area is shown below. (*C*) Percentage of double$^+$ cells relative to mCherry (gray) and ChAT (green) expression (n = 12 slices from 4 mice). (*D*) Schematic representation of a horizontal section indicating the unilateral injection site into MEC (D_1, blue) and LEC (D_2, orange) for retrograde FG (0.5%) tracing experiments. (*E*) Maximum intensity confocal image of MS/DBB showing retrograde FG labeling in ChAT-expressing neurons injected unilaterally in MEC (E_1) and LEC (E_2). Higher magnification of a representative FG$^+$ and ChAT$^+$ cell is shown as below. (*F*) Percentage of double$^+$ cells relative to ChAT expressions after unilateral injection of the retrograde tracer FG into MEC (red; n = 14 slices from 5 mice) and LEC (blue; n = 15 slices from 6 mice). (*G*) Confocal images showing mCherry$^+$ axonal projections in superficial layers of MEC (*Top*) and LEC (*Bottom*). Red dashed lines indicate the border between LI and LII as ascertained based on DAPI staining. (*H*) vAChT punctae are localized within mCherry$^+$ cholinergic axons in MEC (*Top*) and LEC (*Bottom*). Images below show higher magnification of the boxed areas. (*I*) Number of vAChT punctae per micrometer of axon length is shown for MEC (red; n = 32 axon segments from 5 mice) and LEC (blue; n = 20 axon segments from 4 mice). Error bars indicate mean ± SEM. *$P < 0.05$. [Scale bars: (*B* and *E*) 150 µm, (*G*) 50 µm, and (*H*) 10 µm.]

punctae per axon length. Indeed, the synapse density with 2.1 ± 0.1 vAChT punctae/10 μm of axon segment was significantly higher in MEC compared with LEC, with 1.5 ± 0.2 vAChT punctae/10 μm of axon segment (Fig. 1*I*, $n = 32$ axon segments from 5 mice for MEC and $n = 20$ axon segments from 4 mice for LEC, respectively; $P < 0.05$).

Identification and Characterization of Postsynaptic Targets in LI/LII of MEC and LEC. We employed acute slices and performed optogenetic stimulation of MS/DBB-derived cholinergic axons and patch-clamped adjacently located neurons. We recorded from LII EC excitatory and LI/LII EC inhibitory neurons (223 and 289 cells, respectively). In MEC, the four principal cell types—namely, PCs, intermediate pyramidal cells (IMPCs), stellate cells (SCs), and intermediate stellate cells (IMSCs)—were classified based on their intrinsic electrophysiological properties as described before (ref. 13; Fig. S2 *A–F* and Table S1; estimated classification error of ∼5%; see *Materials and Methods*). In LEC, in line with previous reports, the three major principal cell types—that is, PCs, fan cells (FCs), and multiform cells (MFCs)—cannot be distinguished based on electrophysiological properties (Fig. S2 *G–J* and Table S2; estimated classification error of ∼50%) but purely by morphology (11, 14). Therefore, only biocytin-filled and visually identified LEC principal cells were used in this study. LI interneurons can be morphologically segregated into neurogliaform cells (LI NGCs) and single bouquet-like cells (LI SBCs), which constitute the two major cell types (38–40). We could clearly distinguish them based on their intrinsic electrophysiological properties (Fig. S3 *A–C* and Table S3; estimated classification error of ∼5%). As in many other brain areas, EC LII interneurons can be subdivided into three by-and-large nonoverlapping subgroups (13, 41, 42). Their electrical signature corresponds to the expression of distinct neurochemical markers, which are hence considered in this study as putative parvalbumin (pPV^+), putative somatostatin ($pSOM^+$), and putative serotonin receptors ($p5HT_3R$)-expressing interneurons (Fig. S3 *D–G* and Table S4, estimated classification error of ∼2%; see *Materials and Methods*).

Nicotinic Receptor-Mediated Responses Are Elicited in LI and LII $p5HT_3R^+$ Interneurons. Nicotinic acetylcholine receptor (nAChR)-mediated inputs were tested by stimulating septal cholinergic axons with 5-ms LED pulses, while clamping the cells at their approximate resting membrane potential of −70 mV. The nicotinic nature of the resulting excitatory postsynaptic currents (EPSCs) was verified by mecamylamine application (Fig. 2*A*, nonselective nAChR blocker, $n = 17/17$). For some cells, before mecamylamine, we applied CNQX/D-AP5 (glutamatergic receptor antagonists), which did not block the response ($n = 12/12$; amplitude comparison $P > 0.1$). The latency, peak amplitude, rise, and decay time constants for all responding cells in MEC and LEC were 4.1 ± 0.2 ms, 3.2 [1.8, 7.2] pA, 1.5 [1.1, 2.0] ms, and 5.9 [3.5, 8.7] ms, respectively (Fig. 2*B*, reported as mean ± SEM for normally distributed data and median [25th, 75th percentile] for other cases; no difference was observed between MEC and LEC). Cell type-specific response probabilities were statistically estimated using a Bayesian approach and are depicted as violin plots (for details, see *SI Materials and Methods*). Responses were elicited in LI and LII $p5HT_3R^+$ interneurons of MEC (Fig. 2*C*). In LEC, we observed only a few responses in LI/LII interneurons (Fig. 2*C*). Hence septal cholinergic neurons excite LI and LII $p5HT_3R^+$ interneurons via activation of nAChRs.

Septal Cholinergic Neurons Evoke Different Muscarinic Receptor-Mediated Responses. Muscarinic acetylcholine receptor (mAChR)-mediated inputs were tested by stimulating cholinergic axons with ten 5-ms LED stimuli at 5-Hz frequency, while clamping the cells at a subthreshold membrane potential of −50 mV. Two main types of mAChR-mediated responses—namely, hyperpolarizing (Fig. 3A_1) and depolarizing (Fig. 3A_2) responses—were elicited in superficial EC neurons. The resulting EPSCs or IPSCs were verified by bath-application of atropine (nonselective mAChR blocker, $n = 8/8$ for hyperpolarizing and $n = 7/7$ for depolarizing responses). A third type of mAChR-mediated response (biphasic) was rarely observed (Fig. 3A_3, 2/488 cells patched) and was not further analyzed. In MEC and LEC, hyperpolarizing responses were predominantly observed in LII excitatory cells [Fig. 3*C*, excitatory cells (58/151 and 44/98; MEC and LEC) vs. interneurons (5/107 and 2/73): $P < 10^{-10}$ and $P < 10^{-10}$], whereas depolarizing responses were preferentially elicited in interneurons [Fig. 3*D*, interneurons (20/107 and 5/73; MEC and LEC) vs. excitatory cells (0/151 and 0/98): $P < 10^{-8}$ and $P < 0.05$]. Different from other interneurons, pPV^+ interneurons in MEC exhibited a hyperpolarizing and not a depolarizing response ($P < 0.05$). Latency to peak, peak amplitude, and charge for all hyperpolarizing responses were 1.7 [1.2, 1.9] s, 2.8 [2.1, 4.7] pA, and 6.9 [4.1, 13.0] pC (Fig. 3B_1) and for depolarizing responses were 2.8 [1.4, 4.0] s, 2.0 [1.1, 2.9] pA, 4.5 [3.2, 9.7] pC (Fig. 3B_2), respectively ($P < 10^{-3}$, $P < 10^{-3}$, and $P < 0.05$, respectively).

In a subset of experiments, we stimulated with 10 stimuli not only at 5 Hz but also at 2, 10, and 20 Hz to test for a frequency preference (Fig. S4*A*). While peak amplitude plateaued in the theta range, the overall transferred charge did not appear to be dependent on the stimulation frequency (Fig. S4*B*). Thus, we used a simple model (linear rise and decay of each individual EPSC and no short-term plasticity) to predict the observed behavior. As the prediction fit our data nearly perfectly (Fig. S4*B*), it is most likely that there is no strong frequency preference at this synapse.

Notably, previous studies performed in the MEC (36, 37) and other brain regions (43–45) reported opposite results to ours. Exogenous bath application of carbachol (CCh; nonselective AChR agonist) induced slow mAChR-mediated depolarizations, whereas we find that optogenetic stimulation evoked hyperpolarizing responses in excitatory cells. To follow up on this apparent contradiction, we conducted a set of experiments in which we tested optogenetically and CCh-induced responses on the same cell. Nine out of 22 LII MEC excitatory cells showed a mAChR-mediated hyperpolarizing response upon optogenetic stimulation, as opposed to 21 of 22 cells that exhibited mAChR-mediated depolarizations after puff application of 10 mM CCh (Fig. S5). We also tested responses evoked by longer stimulations—that is, 20 Hz for 2 s. All eight tested LII MEC excitatory cells showed a hyperpolarizing response.

MS/DBB Cholinergic Neurons Corelease GABA. Of note, in a substantial fraction of cells (61/488 cells recorded), we observed time-locked fast IPSCs that corresponded most likely to $GABA_A$ receptor ($GABA_AR$) activation. Hence we wondered whether the IPSCs reflected indirect recruitment of local interneurons, in analogy to what was shown for the hippocampus (34), or if MS/DBB cholinergic neurons corelease GABA in EC, as previously suggested in the neocortex (46). We first performed fluorescence in situ hybridization for *Gad1*/*Gad2* and *ChAT* mRNA and found that 88.84 ± 3.73% of MS/DBB cholinergic neurons express *Gad2* (Fig. 4 *A* and *B*, 215 $double^+$ cells from a total of 242 $ChAT^+$ cells in four slices from two mice) but not *Gad1* mRNA (Fig. 4 *A* and *B*, seven $double^+$ cells from a total of 266 $ChAT^+$ cells in four slices from two mice, $P < 0.0001$). Moreover, MS/DBB cholinergic axons expressed vesicular GABA transporter (vGAT) along with vAChT in EC, indicating that GABA may be coreleased (Fig. 4*C*).

We pursued this idea and tested electrophysiologically whether optogenetic stimulation of cholinergic axons in EC directly evokes $GABA_AR$-mediated responses. Cells were voltage-clamped at −50 mV, and a single 5-ms LED stimulus was applied. Resulting IPSCs were preferentially elicited in LI and LII $pSOM^+$ and $p5HT_3R^+$ interneurons (Fig. 4*F*) and were not blocked by CNQX/D-AP5 ($n = 12/12$; amplitude comparison $P > 0.05$), mecamylamine

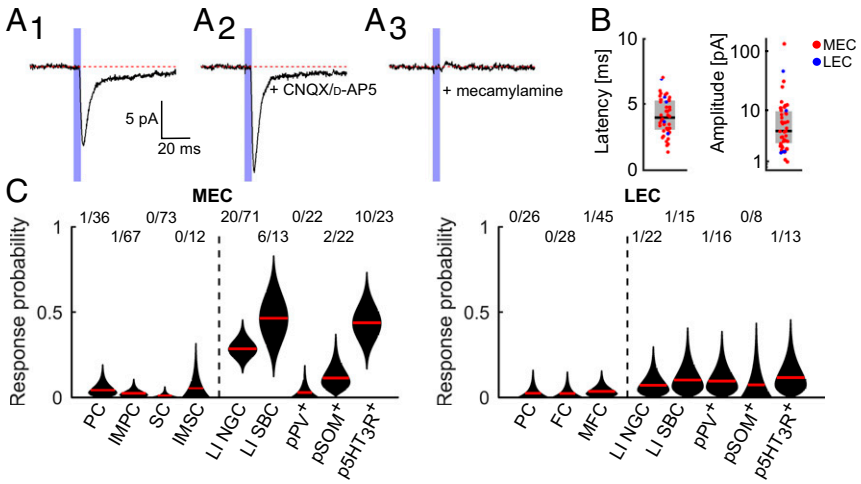

Fig. 2. MS/DBB cholinergic neurons elicit nicotinic receptor-mediated responses in interneurons of EC. (A_1) Representative average current trace of a cell held at −70 mV showing nAChR-mediated EPSC upon single 5-ms LED stimulation. (A_2) Response was not blocked by glutamatergic receptor antagonists (CNQX/D-AP5; $n = 12/12$) (A_3) but was completely blocked by a nonselective nAChR antagonist (mecamylamine; $n = 12/12$). Baselines and LED stimulations are indicated by red dashed lines and blue lines, respectively. (*B*) Box and jittered-dot plots showing the latency and peak amplitude (on a logarithmic scale) of EPSCs elicited in all responding cells in MEC (red) and LEC (blue). (*C*) Cell type-specific responses in MEC (*Left*) and LEC (*Right*) are depicted as violin plots that reflect the number of sampled cells of a given cell type and the number of responding cells within that group of cells (for details, see *SI Materials and Methods*). Red lines indicate the median of the distribution. Vertical dashed line in each plot segregates excitatory (*Left*) from inhibitory (*Right*) cell types. Numbers above the violin plots denote responding and patched cells for every cell type.

($n = 21/21$; amplitude comparison $P < 0.05$, increased amplitude), or atropine ($n = 17/17$; amplitude comparison $P > 0.05$), but only by gabazine (Fig. 4 D_1–D_7, $GABA_AR$ antagonist; $n = 21/21$). In six cells, we tested whether the evoked IPSCs resulted from monosynaptic input. We employed consecutive pharmacological application of tetrodotoxin (TTX; voltage-gated sodium channel blocker) and 4-aminopyridine (4-AP; voltage-gated potassium channel blocker), thereby allowing selective optogenetic depolarization only in ChR2-expressing cells (Fig. 4 D_5 and D_6, 6/6 cells). Finally, $GABA_AR$-mediated responses were verified by gabazine application (Fig. 4D_7, 5/5 cells; one cell was lost during the wash in process of gabazine).

Next, we tested if all recorded responses ($n = 69$) could be subdivided into mono-/polysynaptic responses based on the latency of pharmacologically tested monosynaptic responses ($n = 6$). The mean latency of confirmed monosynaptic inputs was found to be 3.62 ± 0.24 ms and was significantly faster than the overall response latency 4.89 ± 0.18 ms ($P < 0.05$). Moreover, the overall latency distribution showed a partially overlapping bimodal distribution (Fig. 4*E*, Akaike Information Criterion smallest for a bimodal mixed Gaussian model; uni- to decamodal tested). Thus, we used a *k*-mean clustering algorithm (run 1,000 times) to divide the dataset into three groups: putative monosynaptic (41%; 28/69 cells; latency: ≤4.1 ms), putative polysynaptic (28%; 19/69 cells; latency: ≥5.8 ms), and either mono-/polysynaptic (32%; 22/69 cells; latency: between 4.1 and 5.8 ms). The mean latency, rise, and decay time constants, as well as the median peak amplitude, and charge were 3.40 ± 0.10 ms, 2.11 ± 0.26 ms, 9.35 ± 1.01 ms, 6.3 [4.2, 12.3] pA, 0.082 [0.033, 0.137] pC, and 6.53 ± 0.14 ms, 3.70 ± 0.44 ms, 16.93 ± 2.72 ms, 2.7 [2.1, 4.9] pA, 0.037 [0.016, 0.115] pC for putative mono- and polysynaptic responses, respectively. Not only was the latency shorter for putative monosynaptic responses ($P < 10^{-23}$), but the rise and decay time constant and the amplitude were also larger ($P < 0.01$ for all) compared with putative polysynaptic responses. This difference in amplitude might account for the divergent estimates for monosynaptic responses based on the pharmacological approach or latency. Thus, in all pharmacologically tested cells, responses were monosynaptic. However, a bias was introduced, as all six cells had been selected for high amplitude to ensure that the frequently observed small amplitude following 4-AP revival is still detectable. Furthermore, the bimodal latency distribution (Fig. 4*E*) might also reflect presynaptic differences in evoked GABA release from MS/DBB axonal terminals. Using latency as a criterion resulted in an approximation of 41–73%. Additionally, we found a clear tendency of more frequent putative monosynaptic responses in interneurons (22/45) compared with excitatory cells (6/24; $P > 0.05$), which was not the case for putative polysynaptic responses (Fig. 4*G*, $P > 0.25$).

MS/DBB Cholinergic Cells Elicit Differential Responses in Specific EC Neuron Populations. Next, we questioned whether nAChR-, hyper-/depolarizing mAChR-, and mono-/polysynaptic $GABA_AR$-mediated responses occurred within the same neuron. Fig. 5 A_1–A_3 shows sample current traces from a cell in which both nAChR- and $GABA_AR$-mediated EPSC and IPSC, respectively, were observed. Similarly, Fig. 5 *B*–*F* shows sample current traces depicting different response combinations. Note the individual time-locked EPSCs and IPSCs corresponding to nAChR- and $GABA_AR$-mediated responses, respectively, observed at 5-Hz LED stimulation (Fig. 5 A_3, C_3, E_3, and F_3). Fig. 5*G* shows sample current traces of a cell responding to nAChR and $GABA_AR$ activation. At −50 mV, a clear and distinct biphasic response mediated via both nAChR and $GABA_AR$ was observed (Fig. 5G_2). The nAChR-mediated response was abolished not by atropine but only by mecamylamine, and the $GABA_AR$-mediated response was abolished only after the application of gabazine (Fig. 5*G*), thus reconfirming the specificity of the responses. The relative frequency of the different responses elicited in the indicated cell types of MEC and LEC is shown in Fig. 5*H*. The estimated overall response rate of LI (LII) cells was higher than 55% (40%) in MEC and more than 25% (35%) in LEC. Please note the more restricted repertoire of response patterns of excitatory cells in contrast to the large variety of response combinations in interneurons, especially in LI and LII $p5HT_3R^+$ interneurons.

Discussion

Using whole-cell patch-clamp recordings combined with optogenetics, we demonstrate here that the synaptic release of ACh from MS/DBB neurons selectively recruits specific subclasses of superficial EC neurons via the activation of different AChRs. Viral tracing experiments revealed dense MS/DBB cholinergic

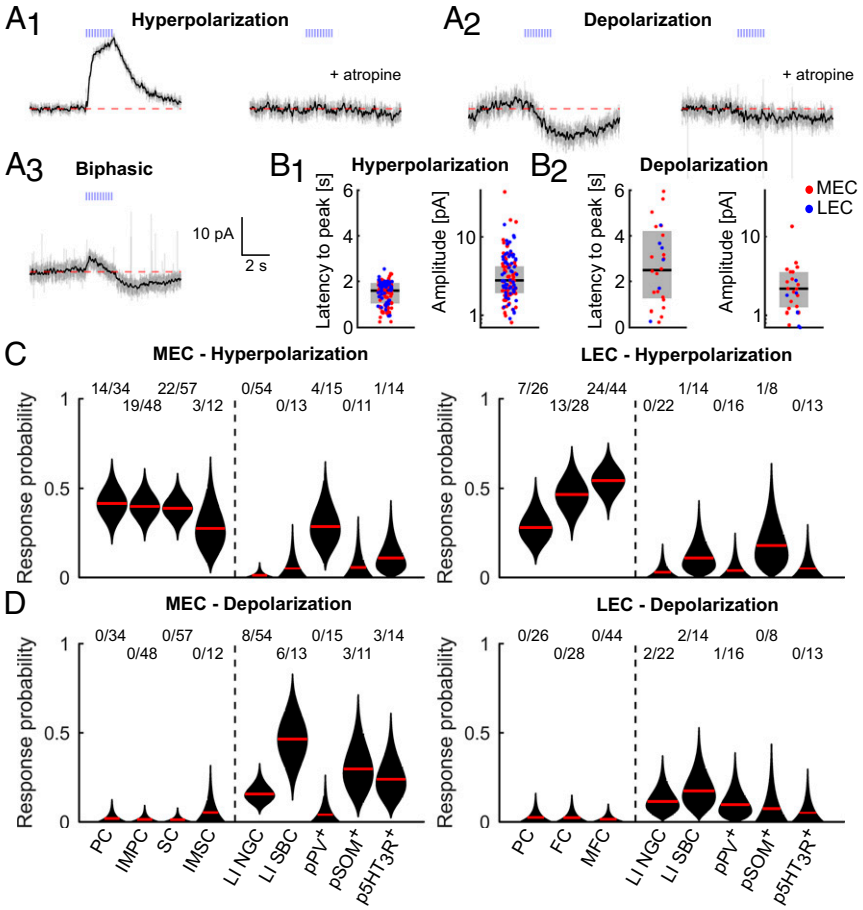

Fig. 3. MS/DBB cholinergic neurons evoke hyperpolarizing or depolarizing muscarinic receptor-mediated responses in a cell type-specific fashion. (*A*) Representative average current traces (gray) of cells held at −50 mV showing mAChR-mediated hyperpolarizing (A_1, *Left*), depolarizing (A_2, *Left*), and biphasic (A_3) response upon ten 5-ms LED stimulations at 5 Hz. In black, Savitzky–Golay-filtered data are shown. Baselines and LED stimulations are indicated by red dashed lines and blue lines, respectively. (A_1, *Right*; A_2, *Right*) Responses were completely blocked by a nonselective mAChR antagonist (atropine; n = 8/8 and 7/7, respectively). (*B*) Box and jittered-dot plots depicting the latency to peak and peak amplitude (on a logarithmic scale) of currents elicited by all MEC (red) and LEC (blue) cells that show either (B_1) a hyperpolarizing response or (B_2) a depolarizing response. (*C* and *D*) Cell type-specific responses are depicted as violin plots that reflect the number of sampled cells of a given cell type and the number of responding cells within that group of cells (for details, see *SI Materials and Methods*). The violin plots indicate the response probability for all target cells in superficial layers of MEC (*Left*) and LEC (*Right*) that show (*C*) a hyperpolarizing response and (*D*) a depolarizing response. Red lines indicate the median of the distribution. Vertical dashed line in each plot segregates excitatory (*Left*) from inhibitory (*Right*) cell types. Numbers above the violin plots denote responding and patched cells for every cell type.

projections in the superficial layers of MEC and to a lesser extent in LEC. Upon optogenetic stimulation of these axons locally in EC, we observed both fast nAChR- and slow mAChR-mediated responses in LI/LII neurons. While $pSOM^+$ and $p5HT_3R^+$ interneurons are depolarized via the activation of mAChRs and/or nAChRs, principal cells and pPV^+ are hyperpolarized via the activation of mAChRs. In a fraction of cholinergic axons, light stimulation led to corelease of GABA, which activates $GABA_A$Rs and evokes inhibitory currents predominantly in LI/LII non-FS interneurons ($pSOM^+$ and $p5HT_3R^+$).

How can the plethora of MS/DBB cholinergic actions affect EC neuronal activity? First, we observed depolarizing nAChR-mediated responses specifically in $p5HT_3R^+$ interneurons and not in pPV^+ and $pSOM^+$ interneurons. This scenario is akin to what was reported for the cortex (45, 47, 48). Notably, nAChR-activated LI and LII $p5HT_3R^+$ interneurons in the cortex were repeatedly shown to inhibit preferentially, if not exclusively, GABAergic interneurons (39, 40, 49). Some studies identified these GABAergic interneurons as $pSOM^+$ (50, 51) or pPV^+ interneurons (48, 52). Based on our results, we envisage a scenario in which LI and LII $p5HT_3R^+$ interneuron activation via nAChRs causes disynaptic disinhibition in neighboring excitatory cells. Given the response kinetics, one can infer that the majority of evoked nicotinic responses were very likely mediated by fast α7-subunit–expressing nAChRs (48).

Second, it is striking that the slow mAChR-mediated depolarizations affect only GABAergic neurons in EC. Cholinergic excitation through mAChRs has been previously reported for hippocampal interneurons (53, 54). Although the function at the network level remains to be established, the implication of mAChRs in theta oscillations was often highlighted in the past (19, 55, 56). In CA1 hippocampal slices, mAChR-induced depolarization in interneurons is essential for generating and sustaining theta oscillations, presumably by changing their active conductances, making them responsive to theta frequency input (57). This in turn would allow interneurons to provide rhythmic inhibition onto PCs (58).

Finally, slow optogenetically induced mAChR-mediated hyperpolarizing responses were predominantly observed in LII excitatory neurons of EC. Of note, the same cells responded to bath/puff application of ACh/CCh with a membrane depolarization, as was often reported by others before (36, 37, 43–45). For instance, Widmer et al. (59) reported that hippocampal interneurons that are unresponsive to synaptically released ACh could be recruited following bath application of CCh. We can only speculate that this

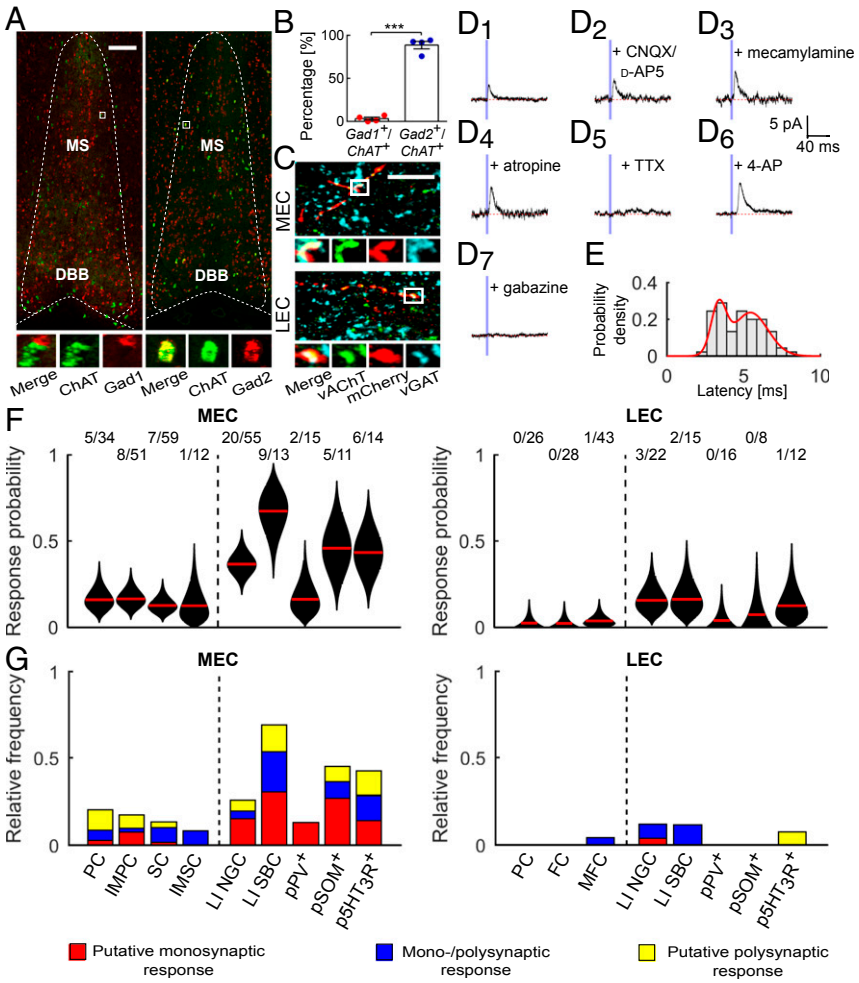

Fig. 4. MS/DBB cholinergic neurons elicit $GABA_AR$-mediated responses in EC neurons. (*A*) Maximum intensity confocal images of fluorescence in situ hybridization showing expression of *Gad1*/*Gad2* (*Left*/*Right*) and *ChAT* mRNA in MS/DBB neurons. Higher magnification images of the boxed areas below show $ChAT^+$ cells that do not express *Gad1* but express *Gad2*. (*B*) Percentage of $ChAT^+$ cells that are $Gad1^+/Gad2^+$ in MS/DBB (n = 4 slices from 2 mice). (*C*) vGAT punctae colocalizing with vAChT punctae inside $mCherry^+$ axonal termini in MEC (*Top*) and LEC (*Bottom*). Images below show higher magnification of the boxed areas. (D_1) Representative average current traces of a cell held at −50 mV showing $GABA_AR$-mediated IPSCs upon single 5-ms LED stimulation. (D_2–D_4) Response was not blocked by CNQX/D-AP5, mecamylamine, and/or atropine but was blocked by application of the $GABA_AR$ antagonist (gabazine, n = 21/21). In six cells, monosynaptic inputs were tested before gabazine application: (D_5) First, the response was abolished by the voltage-gated sodium channel blocker (TTX) and (D_6) subsequently revived by the voltage-gated potassium channel blocker (4-AP). (D_7) The recovered response was again fully blocked by gabazine (n = 5/5). Baselines and LED stimulations are indicated by red dashed lines and blue lines, respectively. (*E*) Histogram of the response latency with a bimodal behavior is shown. Red line is a fit of two weighted Gaussian distributions, which come close to the data. (*F*) Cell type-specific responses in MEC (*Left*) and LEC (*Right*) are depicted as violin plots that reflect the number of sampled cells of a given cell type and the number of responding cells within that group of cells (for details, see *SI Materials and Methods*). Red lines indicate the median of the distribution. Vertical dashed line in each plot segregates excitatory (*Left*) from inhibitory (*Right*) cell types. Numbers above the violin plots denote responding and patched cells for every cell type. (*G*) The relative frequencies of putative mono- (red), mono-/poly- (blue), and putative polysynaptic (yellow) $GABA_AR$-mediated responses, estimated from the latencies of the responses obtained from D_1 experimental conditions, are shown by stacked bar graphs for all cell types in MEC (*Left*) and LEC (*Right*). Error bars indicate mean ± SEM. ***$P \leq 0.0001$. [Scale bars: (*A*) 150 μm and (*C*) 10 μm.]

difference might result from different concentrations of agonist activating predominantly synaptic rather than extrasynaptic mAChRs or due to different ACh sources (e.g., MS/DBB versus local cholinergic interneurons).

The muscarinic depolarizing and hyperpolarizing responses were likely mediated by M1- and M2-type receptors, respectively (60, 61), that, as indicated by our functional results, appear to be differentially expressed in EC interneurons and excitatory cells. The distinct excitatory cell types in the superficial layers of MEC and LEC did not differ with respect to the strength and frequency of hyperpolarizing mAChR-mediated responses. Hence our results cannot explain the in vivo report of stronger theta rhythmicity in PCs compared with that in SCs (62), and other factors must be considered. Furthermore, while we did not observe a robust and direct synaptic mechanism selective for theta, the different kinetics, and therefore timing, of hyperpolarizing excitatory and depolarizing inhibitory cells could potentially enhance and/or restrict the overall network oscillation to a certain frequency (e.g., in the theta range).

There is ample evidence that septal lesions affect not only theta in both EC and hippocampus (24, 25) but also spatial learning (23). Less clear though appears the contribution of the different septal projections in sustaining theta and in particular the mechanisms underlying different forms of theta. MS inactivation and cholinergic blockade led to the differentiation of two forms of theta—namely, urethane- and movement-related theta (21, 63). Theta activity under urethane anesthesia is slower than that seen in freely moving animals, but most importantly, the two forms differ

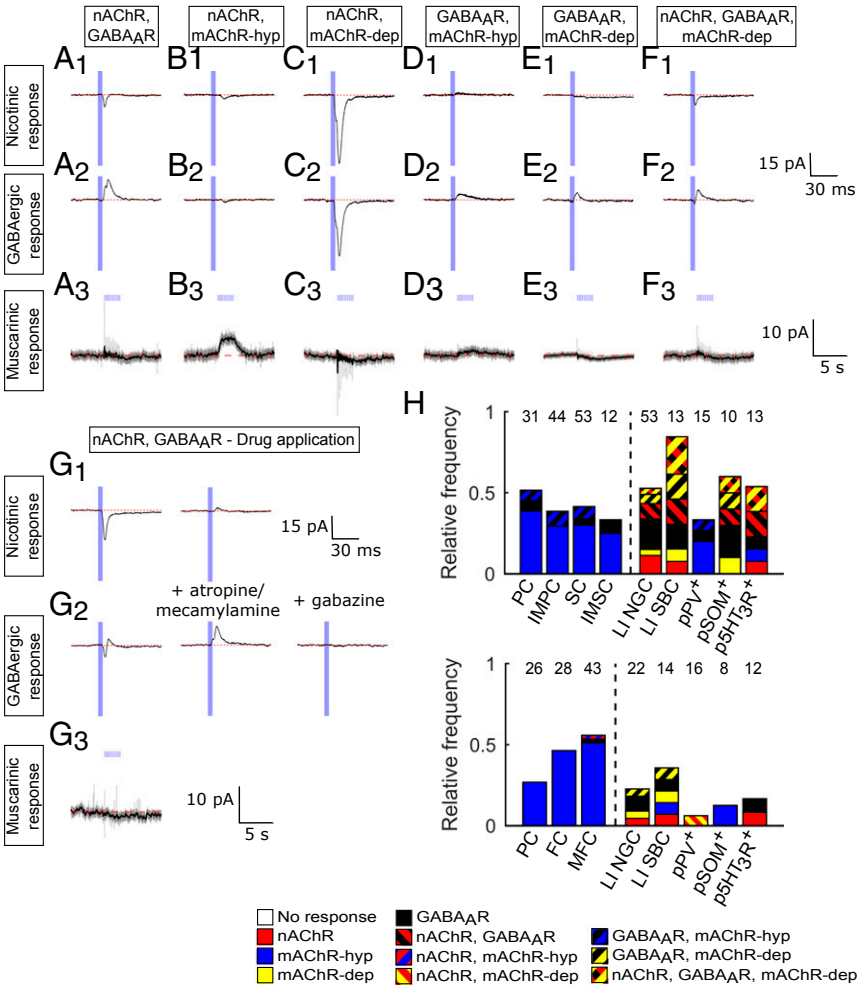

Fig. 5. EC neurons exhibit different receptor-mediated response combinations. (*A–F*) Combinations of nAChR-, $GABA_AR$-, and hyperpolarizing and depolarizing mAChR-mediated responses. Every column depicts measurements from a single cell (*A* and *F*—$p5HT_3R^+$ interneuron; *B*—MFC; *C*—pPV^+ interneuron; *D*—SC; *E*—LI SBC). Representative average current traces of (A_1–F_1) nicotinic (cells held at −70 mV), (A_2–F_2) GABAergic (cells held at −50 mV), and (A_3–F_3) hyperpolarizing or depolarizing muscarinic responses (cells held at −50 mV). In A_3–F_3, Savitzky–Golay filtered data are shown in black. In A_3, C_3, E_3, and F_3, note the individual time-locked EPSCs/IPSCs (seen in overlaid gray traces) corresponding to nAChR/$GABA_AR$-mediated responses. Baselines and LED stimulations are indicated by red dashed lines and blue lines, respectively. (*G*) Representative average current traces of a cell, in which nAChR responses (recorded at −70 mV) and $GABA_AR$-mediated responses (recorded at −50 mV) are elicited. This cell was identified as a $p5HT_3R^+$ interneuron. (G_1) The nAChR-mediated response is not blocked by atropine but is completely blocked by mecamylamine. (G_2) The $GABA_AR$-mediated response is blocked neither by atropine nor by mecamylamine but is blocked by gabazine. (*H*) Stacked bar graphs depicting the relative response frequency of individual cell types, in which either a single response or combinations of responses in superficial neurons of MEC (*Top*) and LEC (*Bottom*) was detected. The number of patched cells for every cell type is mentioned above. $GABA_AR$-mediated responses include both mono- and polysynaptic responses. Responses are specified based on the receptors mediating the corresponding currents. mAChR-dep, depolarizing mAChR-mediated response; mAChR-hyp, hyperpolarizing mAChR-mediated response.

with respect to their response following cholinergic receptor blockade. Atropine, for instance, abolishes urethane-related theta and theta-correlated activity but has only a minor or no effect on movement-related theta (64, 65). Notably, cholinergic and non-cholinergic components of theta have been observed both in hippocampus (31, 64, 65) and in MEC (16, 21).The latter may be supported by septal GABAergic neurons that project to both brain areas. Indeed, pharmacological interventions support the notion that septal GABAergic neurons may contribute to both forms of theta (29, 66, 67). These septal GABAergic neurons can be subdivided into pPV^+ neurons that inhibit preferentially FS interneurons and calbindin-positive neurons that inhibit $pSOM^+$ interneurons (13). We show here that MS/DBB cholinergic neurons can also corelease GABA, thereby adding a third GABAergic input that could potentially be involved in theta rhythmicity. The exact contribution of any of these projections to EC theta remains to be addressed by cell type-specific genetic manipulations.

The finding that some septal neurons corelease ACh and GABA further increases the number of neuronal projections exhibiting a dual neurotransmitter phenotype. The notion of a neuron releasing one fast-acting neurotransmitter has been questioned lately by several studies (46, 68–71). For example, supramamillary nucleus to dentate gyrus and basal ganglia to lateral habenula projections have the capacity to corelease glutamate and GABA (72, 73). More relevant to this study, some basal forebrain cholinergic neurons projecting to the neocortex (46) and hippocampus (74) were demonstrated to corelease GABA and ACh. Here we provide both anatomical and electrophysiological evidence that MS/DBB cholinergic neurons corelease GABA in superficial EC layers. It is very likely that the two neurotransmitters are packed into separate vesicles within the same axonal terminals, as was already shown for the supramamillary nucleus to dentate gyrus projections (72) and the MS to hippocampus projection (74). Even more interesting and functionally relevant is the question of if and how signaling via the

two coreleased neurotransmitters is regulated. It is of note in this context that, at least for the basal ganglia to lateral habenula projection, it was shown that in a mouse model of depression, the balance of coreleased GABA and glutamate is altered and can be restored by antidepressant treatment (73).

Upon activation of cholinergic axons, we observed a similar response profile in LEC, but the response probability was much lower than that in MEC. This is in line with the anatomical difference in our study, as we found fewer cholinergic projections in LEC. Alternatively, AChR expression may be lower in LEC than MEC. In addition, the number of vAChT punctae per micrometer of axon was significantly lower in cholinergic fibers projecting to LEC than that on fibers targeting MEC, indicating fewer ACh release sites. Indeed, anatomical evidence suggests that the extent of cholinergic innervation can vary substantially between different cortical structures (20, 75). Nevertheless, tracing studies revealed an organization of basal forebrain neurons that supports concerted cholinergic regulation of cortical areas that are spatially apart but functionally linked (75). Given the physical closeness of MEC and LEC, but in particular the distinct yet overlapping function of the two brain structures in spatial memory, it is not surprising that upon anterograde labeling of septal cholinergic neurons, we could visualize axons in both areas. At this point, one can only speculate that the quantitative difference in cholinergic innervation might account for the more pronounced theta oscillations and the stronger theta modulation of neurons in MEC compared with LEC (17).

Yet another interesting and related question pertains to the issue as to what extent several downstream areas are simultaneously coordinated by the same septal projections. Thus, in the context of this study, one wonders whether an individual cholinergic projection targets both MEC and LEC. At least for septal GABAergic projections targeting the hippocampus and MEC, we showed that this was the case. Thus, injecting cholera toxin subunit B and FG in the hippocampus and MEC, respectively, we found septal GABAergic neurons that were positive for the two retrograde tracers (13).

In sum, based on viral tracing and optogenetically aided patch-clamp recordings, we here reported and characterized cell type-specific septal cholinergic synaptic input to MEC and LEC. Functional data at this level of analysis—that is, in small circuits—are a prerequisite if we are to understand the action of ACh in these brain areas in vivo. Thus, our data bridge the gap that links neuronal and behavioral levels and provide the necessary information to further probe the contribution and function of different ACh-mediated effects for the generation of rhythmic theta and gamma activity in EC.

Materials and Methods

Experiments were carried out on 8–11-wk-old male wild-type C57/BL6 and ChAT^{Cre} mice [*cre recombinase* expressed in all *choline acetyltransferase* (*ChAT*) positive cells; *Chat*$^{tm2(cre)Lowl}$/J, purchased from The Jackson Laboratory]. Animals were housed in a 12/12 h light/dark cycle with food and water ad libitum. All experiments were performed according to the German protection of animals act and after obtaining approval from the Regierungspräsidium Karlsruhe, Germany. All chemicals were obtained from Sigma-Aldrich unless mentioned otherwise.

Surgical Procedures. Animals were anesthetized with isoflurane, mounted on a stereotaxic apparatus, and kept under isoflurane anesthesia during surgery. Briefly, for AAV injections, AAV-DIO-*ChR2-mCherry* and AAV-DIO-*eGFP* viral vectors were obtained from Penn Vector Core (76, 77). Eight-week-old ChAT^{Cre} mice were subjected to 300 nL viral injections in the MS/DBB as reported before (13). For retrograde tracer injections, 100 nL FG (0.5%) was injected in MEC or LEC of one hemisphere in 8-wk-old wild-type male mice. For this retrograde labeling, surgical procedures were followed as described previously (13, 14). Please see *SI Materials and Methods* for further information.

Immunohistochemistry, Fluorescence in Situ Hybridization, and Reconstruction of Biotin-Labeled Cells. These methods involved standard procedures described in the *SI Materials and Methods*.

Imaging and Image Analysis. Images for immunohistochemistry or in situ hybridization experiments were taken according to a standard protocol using a Zeiss LSM 700 confocal microscope (Carl Zeiss) and analyzed using ImageJ software (ImageJ; US National Institutes of Health). Please see *SI Materials and Methods* for further information.

In Vitro Electrophysiology. Acute coronal, horizontal, and sagittal sections containing MS/DBB, LEC, and MEC, respectively, were 300 μm thick following slicing on a vibratome (Slicer HR2; Sigmann Elektronik). The different planes of sectioning were used to increase the area of the region of interest. Also the axonal projection patterns did not indicate that the plane of sectioning influenced the results (Fig. S1). Sections were incubated at ∼30–32 °C in carbogenated extracellular solution containing (in mM) 125 NaCl, 25 $NaHCO_3$, 1.25 NaH_2PO_4, 2.5 KCl, 2 $CaCl_2$, 1 $MgCl_2$, and 25 glucose. For patch-clamp experiments, cells in EC were viewed with DIC optics, and recordings were performed using HEKA PatchMaster EPC 10 amplifier (HEKA). The injection site and the extent of axonal fibers were visualized based on neuronal mCherry expression. Recording pipettes with a tip resistance of ∼4–6 MΩ were filled with a low Cl^- potassium-based solution containing (in mM) 130 K-gluconate, 10 Na-gluconate, 10 Hepes, 10 phosphocreatine, 4 NaCl, 4 Mg-ATP, and 0.3 GTP, and sometimes 3 mg/mL biocytin with pH adjusted to 7.2 with KOH.

The LED optic fiber (200 μm in diameter, cat. no. M470F1; Thorlabs) was placed above LI to stimulate long-range cholinergic projections with blue light (wavelength, 470 nm). After obtaining a whole-cell configuration, a "test pulse" (TP) and "firing pattern" (FP) were recorded. TP and FP were analyzed offline by a custom-written MATLAB script (The Mathworks) to obtain passive and active properties of the cell.

To test for nicotinic receptor (nAChR)-mediated responses, cells were voltage-clamped at −70 mV and a single 5-ms, 470-nm LED stimulus was applied to depolarize ChR2-containing axonal fibers. To test for muscarinic receptor (mAChR)-mediated responses, cells were voltage-clamped at −50 mV and ten 5-ms LED stimuli at 5 Hz (in some cases also at 2, 10, and 20 Hz) were applied. To test for indirect and direct GABAergic responses upon cholinergic fiber stimulation, cells were voltage-clamped at −50 mV and a single 5-ms, 470-nm LED stimulus was given. Please see *SI Materials and Methods* for further information regarding this section.

Identification of Cell Types. LI/LII EC excitatory and inhibitory neurons were classified based on their morphological characteristics and/or electrophysiological properties similar to previous descriptions (12–14, 38–40, 78). Please see *SI Materials and Methods* for further information.

Violin Plots for the Visualization of Proportions. To get an estimation of the response probability, we used a Bayesian approach. Please see *SI Materials and Methods* for further information.

Quantification and Statistical Analysis. Standard statistical tests were used to analyze the data. Please see *SI Materials and Methods* for further information.

ACKNOWLEDGMENTS. We thank E. Fuchs, A. Caputi, K. Yaqubi, and T. Kuner for helpful discussions; U. Amtmann and R. Hinz-Herkommer for technical assistance; and K. Deisseroth, H. Zeng, and the Allen Brain Institute for making the AAVs available through Penn Vector Core. This work was supported by the Helmholtz Association (PhD scholarship to S.D.), German Cancer Research Center (DKFZ Postdoctoral Fellowship to D.E.K.), Medical Faculty of Heidelberg University (Physician Scientist Fellowship to D.E.K.), and the German Research Foundation [DFG; funding as part of the DFG Collaborative Research Centers (CRC) 1134 (to H.M.)].

1. Steward O (1976) Topographic organization of the projections from the entorhinal area to the hippocampal formation of the rat. *J Comp Neurol* 167:285–314.
2. Witter MP, Groenewegen HJ, Lopes da Silva FH, Lohman AHM (1989) Functional organization of the extrinsic and intrinsic circuitry of the parahippocampal region. *Prog Neurobiol* 33:161–253.
3. Witter MP, Wouterlood FG, Naber PA, Van Haeften T (2000) Anatomical organization of the parahippocampal-hippocampal network. *Ann N Y Acad Sci* 911:1–24.
4. Kerr KM, Agster KL, Furtak SC, Burwell RD (2007) Functional neuroanatomy of the parahippocampal region: The lateral and medial entorhinal areas. *Hippocampus* 17:697–708.
5. Canto CB, Wouterlood FG, Witter MP (2008) What does the anatomical organization of the entorhinal cortex tell us? *Neural Plast* 2008:381243.
6. Hafting T, Fyhn M, Molden S, Moser M-B, Moser EI (2005) Microstructure of a spatial map in the entorhinal cortex. *Nature* 436:801–806.

7. Moser M-B, Rowland DC, Moser EI (2015) Place cells, grid cells, and memory. *Cold Spring Harb Perspect Biol* 7:a021808.
8. Stäubli U, Ivy G, Lynch G (1984) Hippocampal denervation causes rapid forgetting of olfactory information in rats. *Proc Natl Acad Sci USA* 81:5885–5887.
9. Hargreaves EL, Rao G, Lee I, Knierim JJ (2005) Major dissociation between medial and lateral entorhinal input to dorsal hippocampus. *Science* 308:1792–1794.
10. Boisselier L, Ferry B, Gervais R (2014) Involvement of the lateral entorhinal cortex for the formation of cross-modal olfactory-tactile associations in the rat. *Hippocampus* 24:877–891.
11. Canto CB, Witter MP (2012) Cellular properties of principal neurons in the rat entorhinal cortex. I. The lateral entorhinal cortex. *Hippocampus* 22:1256–1276.
12. Canto CB, Witter MP (2012) Cellular properties of principal neurons in the rat entorhinal cortex. II. The medial entorhinal cortex. *Hippocampus* 22:1277–1299.
13. Fuchs EC, et al. (2016) Local and distant input controlling excitation in layer II of the medial entorhinal cortex. *Neuron* 89:194–208.
14. Leitner FC, et al. (2016) Spatially segregated feedforward and feedback neurons support differential odor processing in the lateral entorhinal cortex. *Nat Neurosci* 19: 935–944.
15. Couey JJ, et al. (2013) Recurrent inhibitory circuitry as a mechanism for grid formation. *Nat Neurosci* 16:318–324.
16. Mitchell SJ, Ranck JB, Jr (1980) Generation of theta rhythm in medial entorhinal cortex of freely moving rats. *Brain Res* 189:49–66.
17. Deshmukh SS, Yoganarasimha D, Voicu H, Knierim JJ (2010) Theta modulation in the medial and the lateral entorhinal cortices. *J Neurophysiol* 104:994–1006.
18. Alonso A, García-Austt E (1987) Neuronal sources of theta rhythm in the entorhinal cortex of the rat. I. Laminar distribution of theta field potentials. *Exp Brain Res* 67: 493–501.
19. Buzsáki G (2002) Theta oscillations in the hippocampus. *Neuron* 33:325–340.
20. Mesulam M-M, Mufson EJ, Levey AI, Wainer BH (1983) Cholinergic innervation of cortex by the basal forebrain: Cytochemistry and cortical connections of the septal area, diagonal band nuclei, nucleus basalis (substantia innominata), and hypothalamus in the rhesus monkey. *J Comp Neurol* 214:170–197.
21. Dickson CT, Trepel C, Bland BH (1994) Extrinsic modulation of theta field activity in the entorhinal cortex of the anesthetized rat. *Hippocampus* 4:37–51.
22. Mizumori SJY, Ward KE, Lavoie AM (1992) Medial septal modulation of entorhinal single unit activity in anesthetized and freely moving rats. *Brain Res* 570:188–197.
23. Mitchell SJ, Rawlins JN, Steward O, Olton DS (1982) Medial septal area lesions disrupt theta rhythm and cholinergic staining in medial entorhinal cortex and produce impaired radial arm maze behavior in rats. *J Neurosci* 2:292–302.
24. Brandon MP, et al. (2011) Reduction of theta rhythm dissociates grid cell spatial periodicity from directional tuning. *Science* 332:595–599.
25. Koenig J, Linder AN, Leutgeb JK, Leutgeb S (2011) The spatial periodicity of grid cells is not sustained during reduced theta oscillations. *Science* 332:592–595.
26. Manns ID, Mainville L, Jones BE (2001) Evidence for glutamate, in addition to acetylcholine and GABA, neurotransmitter synthesis in basal forebrain neurons projecting to the entorhinal cortex. *Neuroscience* 107:249–263.
27. Justus D, et al. (2017) Glutamatergic synaptic integration of locomotion speed via septoentorhinal projections. *Nat Neurosci* 20:16–19.
28. Gonzalez-Sulser A, et al. (2014) GABAergic projections from the medial septum selectively inhibit interneurons in the medial entorhinal cortex. *J Neurosci* 34: 16739–16743.
29. Lee MG, Chrobak JJ, Sik A, Wiley RG, Buzsáki G (1994) Hippocampal theta activity following selective lesion of the septal cholinergic system. *Neuroscience* 62: 1033–1047.
30. Brazhnik ES, Muller RU, Fox SE (2003) Muscarinic blockade slows and degrades the location-specific firing of hippocampal pyramidal cells. *J Neurosci* 23:611–621.
31. Vandecasteele M, et al. (2014) Optogenetic activation of septal cholinergic neurons suppresses sharp wave ripples and enhances theta oscillations in the hippocampus. *Proc Natl Acad Sci USA* 111:13535–13540.
32. Dannenberg H, et al. (2015) Synergy of direct and indirect cholinergic septohippocampal pathways coordinates firing in hippocampal networks. *J Neurosci* 35: 8394–8410.
33. Gu Z, Yakel JL (2011) Timing-dependent septal cholinergic induction of dynamic hippocampal synaptic plasticity. *Neuron* 71:155–165.
34. Nagode DA, Tang A-H, Karson MA, Klugmann M, Alger BE (2011) Optogenetic release of ACh induces rhythmic bursts of perisomatic IPSCs in hippocampus. *PLoS One* 6:e27691.
35. Bell LA, Bell KA, McQuiston AR (2013) Synaptic muscarinic response types in hippocampal CA1 interneurons depend on different levels of presynaptic activity and different muscarinic receptor subtypes. *Neuropharmacology* 73:160–173.
36. Klink R, Alonso A (1997) Ionic mechanisms of muscarinic depolarization in entorhinal cortex layer II neurons. *J Neurophysiol* 77:1829–1843.
37. Klink R, Alonso A (1997) Muscarinic modulation of the oscillatory and repetitive firing properties of entorhinal cortex layer II neurons. *J Neurophysiol* 77:1813–1828.
38. Hestrin S, Armstrong WE (1996) Morphology and physiology of cortical neurons in layer I. *J Neurosci* 16:5290–5300.
39. Jiang X, Wang G, Lee AJ, Stornetta RL, Zhu JJ (2013) The organization of two new cortical interneuronal circuits. *Nat Neurosci* 16:210–218.
40. Jiang X, et al. (2015) Principles of connectivity among morphologically defined cell types in adult neocortex. *Science* 350:aac9462.
41. Lee S, Hjerling-Leffler J, Zagha E, Fishell G, Rudy B (2010) The largest group of superficial neocortical GABAergic interneurons expresses ionotropic serotonin receptors. *J Neurosci* 30:16796–16808.
42. Tremblay R, Lee S, Rudy B (2016) GABAergic interneurons in the neocortex: From cellular properties to circuits. *Neuron* 91:260–292.
43. Krnjević K, Pumain R, Renaud L (1971) The mechanism of excitation by acetylcholine in the cerebral cortex. *J Physiol* 215:247–268.
44. Cole AE, Nicoll RA (1984) Characterization of a slow cholinergic post-synaptic potential recorded in vitro from rat hippocampal pyramidal cells. *J Physiol* 352:173–188.
45. Gulledge AT, Park SB, Kawaguchi Y, Stuart GJ (2007) Heterogeneity of phasic cholinergic signaling in neocortical neurons. *J Neurophysiol* 97:2215–2229.
46. Saunders A, Granger AJ, Sabatini BL (2015) Corelease of acetylcholine and GABA from cholinergic forebrain neurons. *eLife* 4:e06412.
47. Porter JT, et al. (1999) Selective excitation of subtypes of neocortical interneurons by nicotinic receptors. *J Neurosci* 19:5228–5235.
48. Arroyo S, Bennett C, Aziz D, Brown SP, Hestrin S (2012) Prolonged disynaptic inhibition in the cortex mediated by slow, non-α7 nicotinic excitation of a specific subset of cortical interneurons. *J Neurosci* 32:3859–3864.
49. Christophe E, et al. (2002) Two types of nicotinic receptors mediate an excitation of neocortical layer I interneurons. *J Neurophysiol* 88:1318–1327.
50. Lee S, Kruglikov I, Huang ZJ, Fishell G, Rudy B (2013) A disinhibitory circuit mediates motor integration in the somatosensory cortex. *Nat Neurosci* 16:1662–1670.
51. Pfeffer CK, Xue M, He M, Huang ZJ, Scanziani M (2013) Inhibition of inhibition in visual cortex: The logic of connections between molecularly distinct interneurons. *Nat Neurosci* 16:1068–1076.
52. Letzkus JJ, et al. (2011) A disinhibitory microcircuit for associative fear learning in the auditory cortex. *Nature* 480:331–335.
53. Pitler TA, Alger BE (1992) Cholinergic excitation of GABAergic interneurons in the rat hippocampal slice. *J Physiol* 450:127–142.
54. Lawrence JJ, Statland JM, Grinspan ZM, McBain CJ (2006) Cell type-specific dependence of muscarinic signalling in mouse hippocampal stratum oriens interneurones. *J Physiol* 570:595–610.
55. Hasselmo ME (2006) The role of acetylcholine in learning and memory. *Curr Opin Neurobiol* 16:710–715.
56. Colgin LL (2016) Rhythms of the hippocampal network. *Nat Rev Neurosci* 17:239–249.
57. Lawrence JJ, Grinspan ZM, Statland JM, McBain CJ (2006) Muscarinic receptor activation tunes mouse stratum oriens interneurones to amplify spike reliability. *J Physiol* 571:555–562.
58. Chapman CA, Lacaille JC (1999) Cholinergic induction of theta-frequency oscillations in hippocampal inhibitory interneurons and pacing of pyramidal cell firing. *J Neurosci* 19:8637–8645.
59. Widmer H, Ferrigan L, Davies CH, Cobb SR (2006) Evoked slow muscarinic acetylcholinergic synaptic potentials in rat hippocampal interneurons. *Hippocampus* 16:617–628.
60. Bonner TI (1989) The molecular basis of muscarinic receptor diversity. *Trends Neurosci* 12:148–151.
61. Brown DA (2010) Muscarinic acetylcholine receptors (mAChRs) in the nervous system: Some functions and mechanisms. *J Mol Neurosci* 41:340–346.
62. Ray S, et al. (2014) Grid-layout and theta-modulation of layer 2 pyramidal neurons in medial entorhinal cortex. *Science* 343:891–896.
63. Jeffery KJ, Donnett JG, O'Keefe J (1995) Medial septal control of theta-correlated unit firing in the entorhinal cortex of awake rats. *Neuroreport* 6:2166–2170.
64. Kramis R, Vanderwolf CH, Bland BH (1975) Two types of hippocampal rhythmical slow activity in both the rabbit and the rat: Relations to behavior and effects of atropine, diethyl ether, urethane, and pentobarbital. *Exp Neurol* 49:58–85.
65. Buzsáki G, Leung LW, Vanderwolf CH (1983) Cellular bases of hippocampal EEG in the behaving rat. *Brain Res* 287:139–171.
66. Smythe JW, Colom LV, Bland BH (1992) The extrinsic modulation of hippocampal theta depends on the coactivation of cholinergic and GABA-ergic medial septal inputs. *Neurosci Biobehav Rev* 16:289–308.
67. Gangadharan G, et al. (2016) Medial septal GABAergic projection neurons promote object exploration behavior and type 2 theta rhythm. *Proc Natl Acad Sci USA* 113: 6550–6555.
68. Ren J, et al. (2011) Habenula "cholinergic" neurons co-release glutamate and acetylcholine and activate postsynaptic neurons via distinct transmission modes. *Neuron* 69:445–452.
69. Hnasko TS, Edwards RH (2012) Neurotransmitter corelease: Mechanism and physiological role. *Annu Rev Physiol* 74:225–243.
70. Root DH, et al. (2014) Single rodent mesohabenular axons release glutamate and GABA. *Nat Neurosci* 17:1543–1551.
71. Tritsch NX, Oh W-J, Gu C, Sabatini BL (2014) Midbrain dopamine neurons sustain inhibitory transmission using plasma membrane uptake of GABA, not synthesis. *eLife* 3:e01936.
72. Boulland J-L, et al. (2009) Vesicular glutamate and GABA transporters sort to distinct sets of vesicles in a population of presynaptic terminals. *Cereb Cortex* 19:241–248.
73. Shabel SJ, Proulx CD, Piriz J, Malinow R (2014) Mood regulation. GABA/glutamate co-release controls habenula output and is modified by antidepressant treatment. *Science* 345:1494–1498.
74. Takács VT, et al. (2017) Synaptic co-transmission of acetylcholine and GABA regulates hippocampal states. bioRxiv:10.1101/193318.
75. Zaborszky L, et al. (2015) Neurons in the basal forebrain project to the cortex in a complex topographic organization that reflects corticocortical connectivity patterns: An experimental study based on retrograde tracing and 3D reconstruction. *Cereb Cortex* 25:118–137.
76. Cardin JA, et al. (2010) Targeted optogenetic stimulation and recording of neurons in vivo using cell-type-specific expression of Channelrhodopsin-2. *Nat Protoc* 5:247–254.
77. Oh SW, et al. (2014) A mesoscale connectome of the mouse brain. *Nature* 508: 207–214.
78. Ascoli GA, et al.; Petilla Interneuron Nomenclature Group (2008) Petilla terminology: Nomenclature of features of GABAergic interneurons of the cerebral cortex. *Nat Rev Neurosci* 9:557–568.